Construction and Building Materials 441 (2024) 137471

Contents lists available at ScienceDirect

Construction and Building Materials

journal homepage: www.elsevier.com/locate/conbuildmat

Geopolymer based on biomass ash from agricultural residues

Zehao Lei, Sara Pavia *

Department of Civil, Structural & Environmental Engineering, Trinity College Dublin, Dublin, Ireland

ARTICLE INFO

Keywords:
Geopolymer
Biomass ash waste
Alkali fusion
Slag
GGBS

ABSTRACT

The expansion of biomass power stations, while advancing carbon neutrality, generates abundant biomass ash waste whose disposal is a challenge. This study uses crop biomass ash (CBA) waste from a power plant to produce geopolymers. Geopolymers are an alternative for reducing CO_2 emissions and resource extraction in construction. This paper studies geopolymers made with raw and alkali-fused CBA. A sodium silicate activator with varying [Na^+] and SiO_2/Na_2O ratios is tested to optimise geopolymerisation. A low fusion temperature (600°C) is used to preserve the environmental credentials of the geopolymers. The geopolymers made with (only) raw CBA have extremely low carbon emissions and environmental impact; they attained the lowest strengths (7.46 and 2.99 MPa-compressive and flexural respectively), a strength range suitable for most construction applications unless higher strength is required for load bearing purposes. Partly replacing the raw ash with slag raised their strength to over 25 MPa and 7 MPa-compressive and flexural respectively. The slag released active Si^{4+}, $Al^{3+}$and Ca^{2+} that participate in the polymerization reaction, forming cements that enhanced strength. Alkali-fusing the ash, even at low temperatures (600°C), enhances reactivity; it breaks down the silicates comprising the ash, providing active radicals that polymerise and form cementing gels that increase strength: the geopolymer made with (only) alkali-fused ash achieved high strengths of 39.35 and 10.74 MPa-compressive and flexural respectively. The geopolymers made with alkali-fused ash and slag consistently show outstanding performance (42–44 MPa compressive strength), and the slag stabilized the system against fluctuations in activator composition. The geopolymers have vitreous structures of cementing gels with high Si^{4+} and Na^+ contents, consistent with an alkaline, silico-aluminate hydrate gel (N-(A)-S-H) which is a typical product of polymerisation. The FTIR results show ample Si-O-Si(Al) bonds in the geopolymer made with alkali-fused CBA. The presence of slag significantly increased the absorption intensity of these bonds, indicating the presence of more abundant C(N)-A-S-H which improved mechanical properties. Incorporating slag vitrifies the geopolymer structure significantly more than alkali-fusing the ash. However, there is no direct proportionality between increasing vitreousness and escalating strength as the crystalline geopolymer (made with alkali-fused CBA only) is nearly as strong as the vitreous, CBA-GGBS geopolymer (39 vs 44 MPa).

1. Introduction

The pursuit of sustainable practices in engineering is a crucial objective in the 21st century. Since the Industrial Revolution, the liberation of productive forces has facilitated the mass production of goods, resulting in widespread availability and reduced costs. However, this progress led to environmental impacts including greenhouse gas emissions, solid waste generation and landfill use which are exacerbated by burgeoning consumer society and industrial activity [1]. With the global population projected to continuously grow, the demand for resources will intensify, challenging the finite Earth's resources which are insufficient to support exponential economic and population growth. In this context, environmental pollution and global resource scarcity are escalating challenges. The manufacturing industry must navigate environmental regulations, resource price volatility and potential shortages while maintaining operations [1].

The circular economy (CE) is a viable approach to align economic growth with environmental sustainability [2]. CE emphasizes circular flows of substances and multi-stage use of raw materials and energy sources [3,4]. In the construction sector (which consumes nearly 40 % of total energy production and emits abundant CO_2 emissions, with cement production alone accounting for 8 % of global CO_2 emissions annually) there is a pressing need to develop alternative solutions [5] to support sustainable building practices and align with sustainable development

* Corresponding author.
E-mail address: PAVIAS@tcd.ie (S. Pavia).

https://doi.org/10.1016/j.conbuildmat.2024.137471
Received 17 May 2024; Received in revised form 18 June 2024; Accepted 12 July 2024
Available online 24 July 2024

goals.

Biomass power generation emerged in the 1970s, primarily driven by the global oil crisis, which compelled many countries to explore renewable energy sources [6,7]. By the 1990s, this technology had become widespread in the United States and Europe [8–10]. Currently, amidst increasing demands for carbon neutrality, biomass power generation is regaining prominence due to its carbon-neutral potential [11,12]. The carbon dioxide released during the combustion of biomass is approximately equal to that absorbed during its photosynthesis, rendering the net carbon emissions from biomass power generation nearly zero [13]. Additionally, biomass has a very low sulphur content, resulting in minimal sulphur emissions [14]. Thus, substituting traditional coal-fired power with biomass can significantly enhance environmental quality and mitigate the greenhouse effect. Despite these advantages, the generation of biomass ash (BA) waste remains an environmental concern. Approximately 95–97 % of global bioenergy is produced through biomass combustion, generating massive amounts of BA [13,15]. With the world's biomass potential for energy applications estimated at about 7 billion tonnes annually and an average ash yield of 6.8 %, it is estimated that around 476 million tonnes of BA will be produced each year worldwide [14]. This raises critical questions on the management and utilization of such large volume of biomass ash in sustainable ways.

This study uses crop biomass ash (CBA) waste from power plants to produce geopolymers. Geopolymers are recognized as a practical solution for reducing CO_2 emissions and resource extraction in construction [16]. They are a sustainable alternative to traditional cement, featuring greater energy efficiency, lower carbon emissions and the incorporation of raw materials including industrial waste [17]. Geopolymerization involves the dissolution of aluminosilicate materials in concentrated alkaline solutions which results in the release of free silica and alumina radicals that can later polymerise. The subsequent condensation of alumina and silica units creates inorganic geopolymer gels which harden into robust, three-dimensional, silica-aluminate networks that constitute the geopolymer [18].

CBA is an aluminosilicate waste, rich in silicon and aluminium. Due to an undesirable thermal history during power generation, the CBA is highly crystalline. High crystallinity can hinder reactivity which limits the CBA application in geopolymer and cement technology. Attempts to recover CBA in two-component geopolymer are still lacking.

Other biomass ashes such as rice husk ash (RHA) and sugar cane bagasse ash (SCBA) are typically burned in uncontrolled conditions or at lower temperatures, therefore their reactivity varies and can be high. Hence, they can be used in cement and geopolymer technology, as precursors or supplementary cementitious materials – SCMs [19–24]. As natural materials, ashes are subject to variability. Some SCBAs show poor reactivity due to lack of control over their production parameters which restricts their use [22,25,26] while other SCBAs are notably pozzolanic reaching an MI=1.5 and twice the strength of a reference lime mix [27,28]. Similarly, some RHAs of high specific surface area, produced at low temperatures of 400–500°C are highly reactive, and significantly speed up the setting and strength development [19,26,29]

Previous research demonstrated that the CBA in this research has low pozzolanic activity [30]. To expand the possibilities of CBA in geopolymer synthesis, an appropriate treatment to increase its reactivity is necessary. Thermal treatment is generally effective to enhance the reactivity of clay-based materials such as calcined clays [31] and metakaolin [32]. However, for highly crystalline and thermodynamically stable minerals, simple calcination does not destroy the crystalline structure, such is the case of the zeolite comprising spent FCC catalysts [33]. More innovative ways to disrupt the crystal structure in silicate wastes to increase their activity are therefore needed.

Alkali fusion is an effective method to enhance the reactivity of silicoaluminate minerals and wastes by disrupting their inert crystals into active phases such as soluble silicates [34–36]. Alkali fusion was initially employed to digest insoluble substances for constituent analysis, such as in gas chromatography [37,38] and ICP-MS [39,40]. Subsequently, it has been used for synthesizing zeolites [41,42] and extracting valuable elements from crystalline wastes [43,44]. Although alkali fusion has been proven successful in improving reactivity, its effect on geopolymerisation still lacks investigation. Moukannaa et al. [45] found that alkali-fusion decomposed illite, palygorskite and dolomite thereby increasing the reactivity of mine tailings. However, whether the alkali fusion method is equally effective for highly crystalline silicate wastes still requires further study. This research uses raw and alkali-fused CBA waste to produce geopolymers. It is hoped that the fusion breaks down the crystalline fraction in the CBA to produce radicals, active in polymerisation reactions, that enhance the production of cementing gels and raise strength development.

Activators are crucial in geopolymerization, with Na_2SiO_3 (sodium silicate) and NaOH (sodium hydroxide) being the most common. NaOH raises alkalinity, assisting the dissolution of precursors [46] while Na_2SiO_3 provides lower alkalinity over longer periods [47,48] and soluble silicate that fosters the formation of aluminosilicate gels which enhance strength and durability [49–51]. The activator concentration controls the hydrolysis of aluminosilicate materials [52,53]. It is well known that low concentrations can lead to inadequate dissolution, resulting in reduced polymerization and weaker mechanical properties; and conversely, extreme concentration can cause efflorescence, brittleness, excessive porosity, and lower strength and durability. The activator in this research was made with solid NaOH and a sodium silicate solution. The activator's molar ratio (SiO_2/Na_2O) and Na^+ concentration are adjusted to provide a range of differing alkalinities and soluble silicate contributions.

Raw and alkali-fused CBA are used, either alone or combined with GGBS, to develop geopolymers. The slag is highly vitreous and hence a great source of active silica and calcium that promote the formation of cementing hydrates [54]. This study measures the workability and mechanical properties of the geopolymers and studies the composition and microstructure of the resulting geopolymer cements with XRD, FTIR and SEM/EDX to determine the best composition and activation conditions.

2. Materials and methods

2.1. Materials

The biomass ash used in this study was supplied by Beijing Zhineng Xiangying Energy Conservation and Environmental Protection Technology Company. This biomass ash, designated as crop biomass ash (CBA), is a bottom ash derived from the combustion of local agricultural residues, including rice husks and maize stalks, for power generation. The stable source of biomass and the consistent incineration process ensures the uniformity of the composition and properties of the resultant ash. The exact combustion temperature of the ash is not known but it is likely to be within the typical range for wood-chip boilers of 540–600°C for the initial burn which releases gases, and up to 1200°C for the reburn of the gases in the calcination chamber. Therefore, internal temperatures usually range between 500°C and 1200°C [55]. The CBA, as received from the power plant, comprises large, sintered masses and fine powder. To achieve homogeneous powders, the CBA was ground in a ball mill for two hours. Ground granulated blast furnace slag (GGBS) was used as a source for silica and calcium. The slag used is highly vitreous and hence a great source for active silica and calcium [54]. The chemical compositions of CBA and GGBS were analysed with X-ray fluorescence spectrometry (XRF) and the particle size distribution was measured by laser diffraction. The results appear in Table 1. The SiO_2/Al_2O_3 ratio of CBA and GGBS are calculated at 5.32 and 3.51 respectively.

The morphology of CBA was studied with a scanning electron microscope (SEM) and it is presented in Fig. 1. Most of the CBA particles are porous and angular. A small number of solid particles with smooth surfaces were also observed which are presumed to be silt contaminants.

Table 1
Properties of CBA and GGBS.

	CBA	GGBS
Chemical composition by XRF (wt%)		
SiO_2	68.40	36.5
Al_2O_3	12.85	10.4
Fe_2O_3	5.01	0.7
CaO	1.75	42.4
MgO	1.24	8.1
Na_2O	1.86	0.5
K_2O	3.57	-
Cr_2O_3	0.01	-
TiO_2	0.75	0.5
P_2O_5	0.38	0.42
SrO	0.02	-
BaO	0.07	-
LOI	3.63	-
Particle size distribution and specific surface area		
D_{50} (μm)	62.3	11.67
SSA (m^2/kg)	317.5	1340

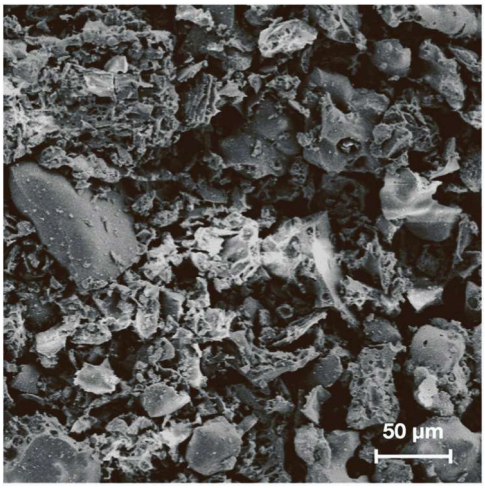

Fig. 1. SEM micrograph of the particles comprising the CBA.

The lack of organic matter is deemed to be due to the combustion and mechanical grinding of the biomass. The porous and angular structure of the particles is comparable to other ashes in the literature [26,28]. This structure of high porosity and high specific surface area is likely to favour reactivity and may increase water demand, affecting the rheology of the resultant materials.

The mineral composition of CBA, analysed with X-ray diffraction (XRD), appears in Fig. 2. The analysis revealed a high crystallinity which can be attributed to a combination of high calcination temperature and soil contamination. The main crystalline phases are quartz and albite. They appear alongside a notable hump centred at 25° 2θ which indicates the presence of amorphous content. The high crystallinity suggests a potential low reactivity for the ash.

As aforementioned, alkali fusion was employed to enhance CBA reactivity. The alkali fusion process involved mixing ground CBA powder with 25 % sodium hydroxide and heating at 600°C for two hours. The mineral composition of the alkali-fused CBA is included in Fig. 2. Alkali-fusion, decomposed the quartz and albite comprising the raw ash, transforming them into reactive sodium aluminosilicate phases including **A_S:** Sodium aluminosilicate, $Na_{1.15}Al_{1.15}Si_{0.85}O_4$, PDF 04–010–3962 and **$A_{S2}$:** Sodium aluminosilicate, $Na_{0.98}Al_{0.98}Si_{1.02}O_4$, PDF 04–016–6555 (Fig. 2).

The FTIR spectra of raw and alkali-fused CBA revealed microstructural alterations caused by the alkali-fusion process (Fig. 3). The main band in raw CBA, located between 820 cm^{-1} and 1264 cm^{-1}, is attributed to the stretching vibrations of Si-O-Si(Al). After the alkali-fusion process, this band shifts to a lower wavenumber, suggesting that the original highly cross-linked Si chains were disrupted, producing low-aggregation Si units and possible Al substitutions [56].

The alkali activator was prepared using solid sodium hydroxide (99 % purity pellet), sodium silicate solution (27.8 wt% SiO_2, 8.5 wt% Na_2O, 63.7 wt% H_2O) and distilled water. The modulus (Ms = SiO_2/Na_2O molar ratio) of the activator ranged from 1.0 to 1.4. Varying amounts of NaOH were used in the design to achieve the required modulus. The concentration of Na^+ was set between 8 and 1.2 mol/L and controlled by adding distilled water.

2.2. Methods

2.2.1. Geopolymer synthesis

To evaluate the potential of CBA as a precursor for geopolymer

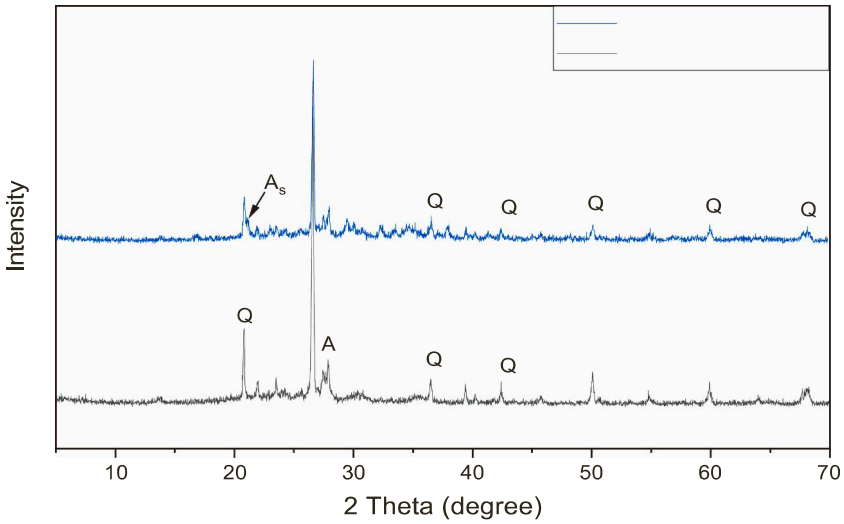

A_S: Sodium aluminosilicate , $Na_{1.15}Al_{1.15}Si_{0.85}O_4$, PDF 04-010-3962
A_{S2}: Sodium aluminosilicate , $Na_{0.98}Al_{0.98}Si_{1.02}O_4$, PDF 04-016-6555
Q: Quartz, SiO_2, PDF 04-016-2085 **A:** Albite, $NaAlSi_3O_8$, PDF 01-072-8434

Fig. 2. Mineral composition of raw and alkali-fused CBA.

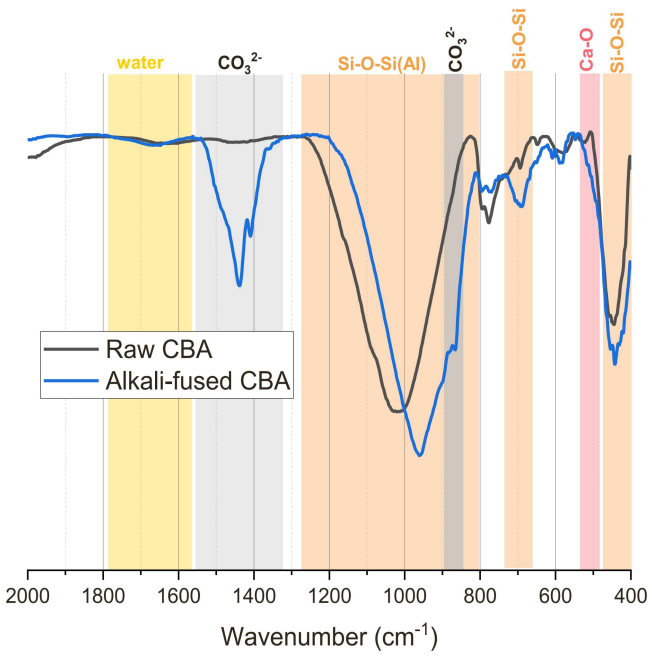

Fig. 3. FTIR spectra for the raw and alkali-fused CBA.

development, several variables were investigated including the ideal activator composition and the optimum ratio of CBA to GGBS. Geopolymers with varying compositions and activators were fabricated and tested. The detailed composition of the specimens is given in Table 2. All raw materials were combined with the activator using a mechanical mixer for 10 minutes. The resulting slurry was then cast into steel moulds measuring 40x40x160 mm. The specimens were demoulded after 24 hours, and subsequently cured in controlled conditions at a temperature of 20±2 °C and 60±5 % relative humidity.

2.2.2. Mechanical properties and workability

The compressive and flexural strengths of the CBA geopolymers were evaluated using a Zwick loading machine, according to the EN 196–3:2016 standard, after a curing period of 28 days. The reported values are the arithmetic mean of 4–6 specimens. The workability of the geopolymers was assessed by measuring the initial flow diameter with a flow table according to European standards (EN 459–2).

2.2.3. Characterization techniques

The mineral composition of the raw materials and the resulting geopolymer cements were studied by X-ray diffraction (XRD) with the powder method, using a Bruker D500 apparatus with a 2θ range between 5° and 70°. The morphology and composition of the geopolymer were investigated by scanning electron microscopy (SEM) with a TESCAN MAIA3LMH apparatus equipped with an Octane Super EDX detector. The function groups of the geopolymer cements were analysed with Fourier-transform infrared spectroscopy (FTIR). The analyses were carried out using a PerkinElmer Spectrum 100 FTIR apparatus equipped with an ATR accessory and a one-bounce diamond/KRS5 top plate.

3. Results and discussion

3.1. Performance of CBA-based geopolymer

The flow table test displayed the spread of the geopolymers, upon removing the mould after 15 flow table jolts, as a measurement of the geopolymer workability. The initial flow of the different formulations was measured, at constant water content, to estimate the geopolymer workability and how the different proportions ash/slag affect water demand. Fig. 4 illustrates the test assemblage and measurement. The workability results appear in Fig. 5. The low flowability of the geopolymers made with ash only agrees with the high porosity and specific surface area of their particles observed with SEM (Fig. 1). As highlighted by former authors [57,58] a greater specific surface area raises water demand, and the material requires a greater amount of water to produce a given workability (or flow). The geopolymer made with 100 % CBA, both raw and alkali fused, has low workability, showing the lowest initial flow diameters of 100 mm. Similar findings are reported for comparable materials such as rice husk ash (RHA)-based geopolymers [59–61]. RHA shares a similar morphology with CBA due to their analogous origin. The CBA absorbs significant water quickly due to the porous nature of its particles, diminishing flowability. The incorporation of GGBS improves the flowability of the CBA geopolymer mortars agreeing with former authors who evidenced that the dense GGBS

Table 2
Mix design of CBA-based geopolymer. w/b = 0.6. C = CBA; fC = alkali fused CBA; G = GGBS.

Group	Notation	Precursor g			Activator		Sand g
		CBA		GGBS	Na^+ Concentration mol/L.	SiO_2/Na_2O ratio	
		C	fC				
A	100 C	400			10	1.2	1200
A	100 fC		400		10	1.2	
B	70 C 30 G	280		120	10	1.2	
B	70 fC 30 G		280	120	10	1.2	
B	50 C 50 G	200		200	10	1.2	
B	50 fC 50 G		200	200	10	1.2	
B	30 C 70 G	120		280	10	1.2	
B	30 fC 70 G		120	280	10	1.2	
C	100fC/8/1.0		400		8	1.0	
C	100fC/8/1.2		400		8	1.2	
C	100fC/8/1.4		400		8	1.4	
C	100fC/10/1.0		400		10	1.0	
C	100fC/10/1.2		400		10	1.2	
C	100fC/10/1.4		400		10	1.4	
C	100fC/12/1.0		400		12	1.0	
D	30 fC 70 G/ 8/ 1.0		120	280	8	1.0	
D	30 fC 70 G / 8/ 1.2		120	280	8	1.2	
D	30 fC 70 G / 8/ 1.4		120	280	8	1.4	
D	30 fC 70 G / 10/ 1.0		120	280	10	1.0	
D	30 fC 70 G / 10/ 1.2		120	280	10	1.2	
D	30 fC 70 G / 10/ 1.4		120	280	10	1.4	
D	30 fC 70 G / 12/ 1.0		120	280	12	1.0	

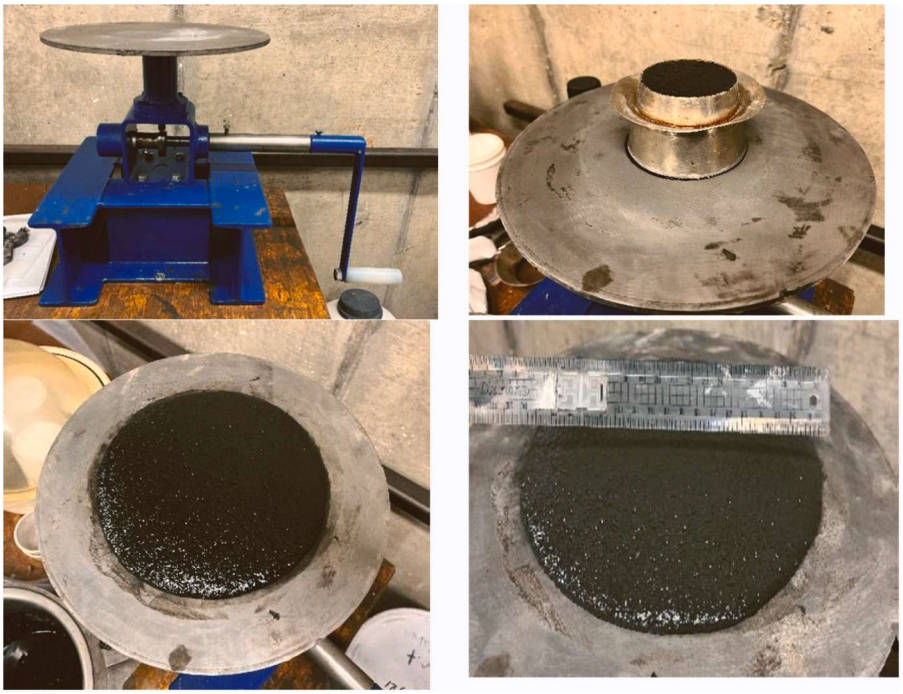

Fig. 4. Test assemblage and measurement of geopolymer workability using the initial flow test. Top: flow table and conical mould. Bottom: Lifting of the mould and measurement of the initial flow.

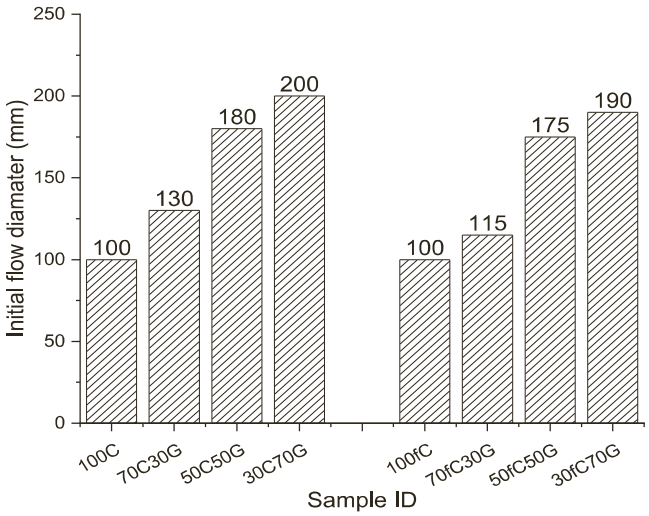

Fig. 5. Flowability of CBA and CBA-GGBS geopolymers.

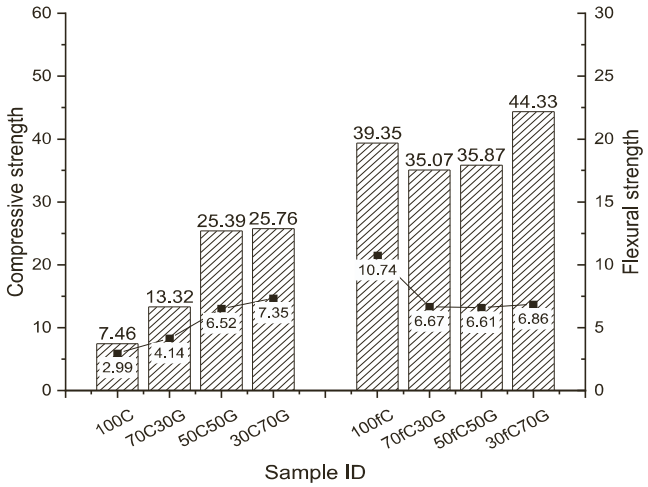

Fig. 6. Effect of alkali-fusing the CBA on the mechanical performance of CBA and CBA-GGBS geopolymers. Groups A and B in Table 2: $[Na^+]$ = 10 and Ms = 1.2.

particles tends to enhance the workability of composites [58].

On the contrary, alkali diffusion lowers the flowability of the geopolymer. As aforementioned, alkali fusion involved heating (at 600°C) a mix of CBA and 25 % NaOH. When adding water to the fused CBA, sodium residues like sodium carbonate form by carbonation with atmospheric carbon, and these crystals impede flow lowering workability.

The strength of the CBA geopolymers at 28d appears in Fig. 6. The **geopolymers made with alkali-fused CBA** are stronger than their raw CBA counterparts. The inferior strength of the raw CBA geopolymers is due to the limited dissolution of the silicate crystals (quartz and albite) comprising the CBA (Fig. 2). The importance of dissolving the precursor, to provide silicon and aluminium species essential for subsequent gelation and polymerization reactions, is well established in geopolymer technology [17]. Quartz and albite are highly stable chemically and thermally and require strong acidic/alkaline conditions to dissolve. Therefore, within the alkalinity range of the activator in this research, the silicates comprising the raw CBA remain mostly stable, contributing little to polymerisation. However, alkali fusion breaks down the CBA's silicates releasing active silica radicals that participate in polymerisation reactions forming cementing hydrates that increase the geopolymer strength. The **geopolymers made with raw CBA** increase strength with increasing CBA substitution with GGBS. Therefore, the active silica and calcium released by the slag participates in polymerization reactions and hydrate formation increasing strength. The results also indicate that alkali fusing the ash enhances strength more efficiently that replacing ash with slag. Hence, alkali fusion is a more effective method to provide active radicals for the polymerization and hydrate formation than increasing slag content.

As aforementioned, the **raw CBA geopolymers** increase strength

with increasing CBA substitution with GGBS. After 28 days, the geopolymer made with as alone (100 % raw CBA - 100 C) yields the lowest strengths of 7.46 MPa and 2.99 MPa - compressive and flexural respectively; but replacing ash with slag improved mechanical performance: replacing 30 % of CBA with GGBS increased strengths to 13.32 MPa and 4.14 MPa - compressive and flexural respectively, corresponding to improvements of 78.55 % and 38.46 %; and at 50 % GGBS replacement, the strengths rose to 25.39 and 6.52 MPa respectively. However, beyond this threshold, increasing GGBS (to 70 %) only yields a marginal strength enhancement, with values of 25.76 MPa and 7.35 MPa respectively.

The **geopolymers made with alkali fused CBA** are stronger than their raw CBA counterparts. The 100 % alkali fused CBA geopolymer (100fC) achieved strengths of 39.35 and 10.74 MPa - compressive and flexural respectively, improving by 427.48 % and 259.20 % respectively compared to the raw CBA geopolymer. Replacing alkali-fused CBA with GGBS slightly lowers mechanical strength: at 30 % GGBS content, strength decreased from 39.35 to 35.07 MPa and escalating GGBS to 50 % did not significantly alter performance. However, at 70 % GGBS content, a notable strength improvement occurs at 44.33 MPa. The strength increase triggered by GGBS substitution is more pronounced in the raw CBA group, indicating that the synergistic effect between GGBS and CBA becomes weaker when the CBA is fused.

The geopolymers made with alkali-fused CBA (100fC and 30fC 70 G groups) were selected to further investigate the optimum activator composition due to their excellent mechanical performance. The **effect of the activator composition,** including Na^+ concentration and SiO_2/Na_2O, on mechanical performance appears in Fig. 7. The geopolymers made with activators of ratio SiO_2/Na_2O=1.0 produced flash set regardless of the [Na^+]. Flash set produced premature hardening and lack of workability so that strength could not be measured. Flash set of geopolymer is rarely reported and, when reported, it is linked to high pH and high-calcium (Class C) fly ash-based geopolymers [62–64]. In contrast, in this research, flash set occurred at both high-calcium (Group D- 70 %GGBS) and low-calcium content (Group C- 100 fC), when the activator SiO_2/Na_2O was 1.0. The relatively low ratio $SiO_2/Na_2O = 1.0$ implies high alkalinity. A clear pattern exists where the most alkaline activator ($SiO_2/Na_2O = 1.0$) triggered the flash set of the geopolymer (Fig. 5). The high alkalinity caused rapid precursor dissolution which produced flash set.

The geopolymers made with alkali-fused CBA (100fC group) performed best when the SiO_2/Na_2O was 1.2. Increasing silica content beyond this ratio worsened mechanical performance, suggesting that an excessive SiO_2/Na_2O ratio provides insufficient alkalinity for effective precursor dissolution while providing excess soluble silica. This imbalance likely promotes polymerization of silica species within the activator, hindering the dissolution of the precursor. The results also indicate that maintaining the SiO_2/Na_2O ratio while increasing the Na^+ concentration of the activator slightly improves strength development.

The geopolymers made with alkali-fused CBA and GGBS (30fC70G group) constantly display an outstanding mechanical performance (42–44 MPa compressive strength at 28 d.), and variations in the activator composition had no significant impact on mechanical performance, with changes in strength under 10 %. The presence of GGBS significantly enhanced strength and stabilized the system against fluctuations in activator composition. Unlike the dramatic strength reductions seen in the low-calcium system (100fC group) when lowering alkalinity and increasing the silica content beyond $SiO_2/Na_2O = 1.2$, the strength of the 30fC70G geopolymers remains stable over the whole range of ratios investigated (1.0–1.4) and increasing [Na^+] does not significantly impact strength.

3.2. Microstructure of the CBA-based geopolymer

The mineral compositions of CBA and CBA-GGBS geopolymers appear in Fig. 7. The raw CBA geopolymer (100 C) includes quartz and albite (Fig. 8a). These are unreacted remnants of the silicates originally comprising the CBA. The intensity and sharpness of the peaks suggest significant crystalline content which may contribute to the strength to some extent but does not form significant cementing gels that induce high strength, agreeing with the lower strength above (7.46 MPa at 28d.). The alkali-fused CBA geopolymer (100fC) (Fig. 6a) displays less crystallinity and a more amorphous structure that correlates with the formation of cementing gels characteristic of geopolymers and agrees

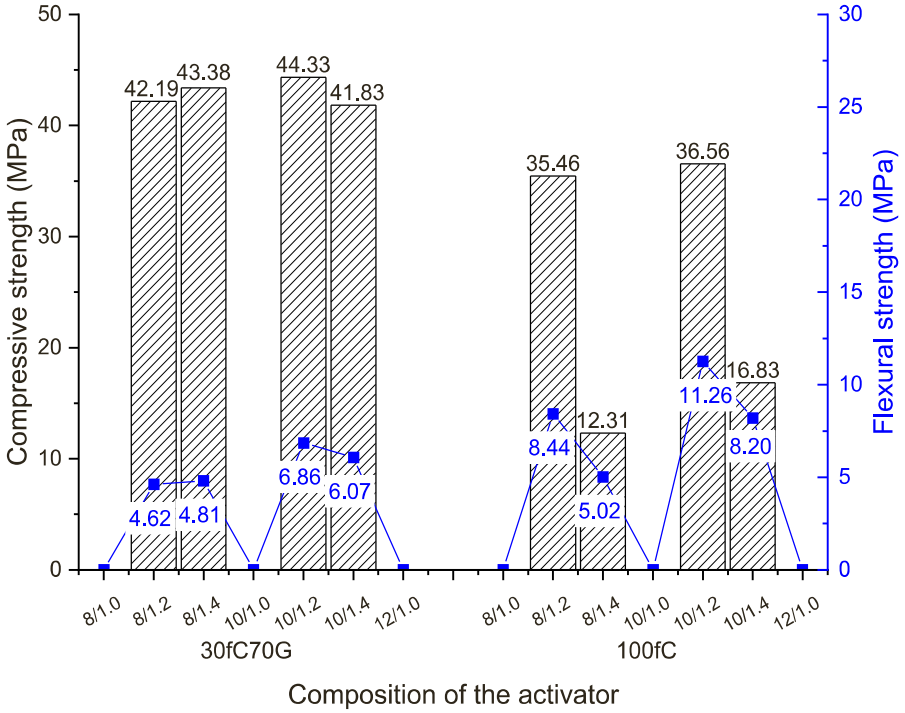

Fig. 7. Effect of activator's alkalinity and silica modulus on the mechanical performance of CBA and CBA-GGBS geopolymers. Groups C and D in Table 2.

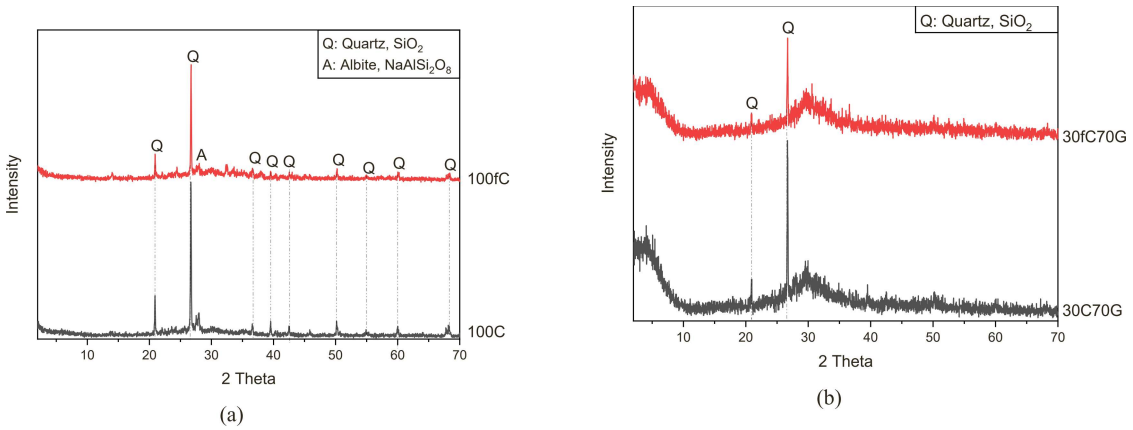

Fig. 8. Mineral composition of (a)100 % CBA and (b) CBA-GGBS geopolymer. Top: alkali-fused CBA geopolymer. Bottom: raw CBA geopolymer.

with the greater strength seen above (39.35 MPa at 28 d.).

Replacing CBA with GGBS significantly transforms the geopolymer structure from crystalline into amorphous, regardless of the CBA being fused or not (Fig. 8b). The amorphous structure is typical of geopolymers and alkali-activated materials [56]. The significant amorphous content represents an ample cementing gel phase which should enhance mechanical performance. However, the results suggest that the geopolymer structure (i.e. crystallinity vs amorphousness) does not mirror its mechanical performance: despite the abundant amorphous cement produced by the GGBS in the 30 C 70 G and 30fC 70 G geopolymers (70 % GGBS substitution), their strengths (13.32 MPa and 35.07 MPa respectively) are lower than the strength of the crystalline geopolymer (100fC) which reached 39.35 MPa. According to the amorphous content evidenced in the XRD traces (Fig. 8) both alkali-fusing the ash and incorporating slag vitrify the geopolymer structure but GGBS vitrifies the structure to a much greater extent than alkali fusion.

The reduction of the intensity of the quartz peak in the XRD traces corresponding to the alkali-fused geopolymers (Fig. 8a, b) indicates that alkali fusion at low temperature (600°C) breaks tectosilicate structures as strong and stable as quartz.

The microstructure of the geopolymers appears in Figs. 9 and 10. Despite the drastic change in mineralogy and microstructure (from crystalline into amorphous when GGBS was added) evidenced with XRD, the SEM analyses show vitreous geopolymer cements in all the

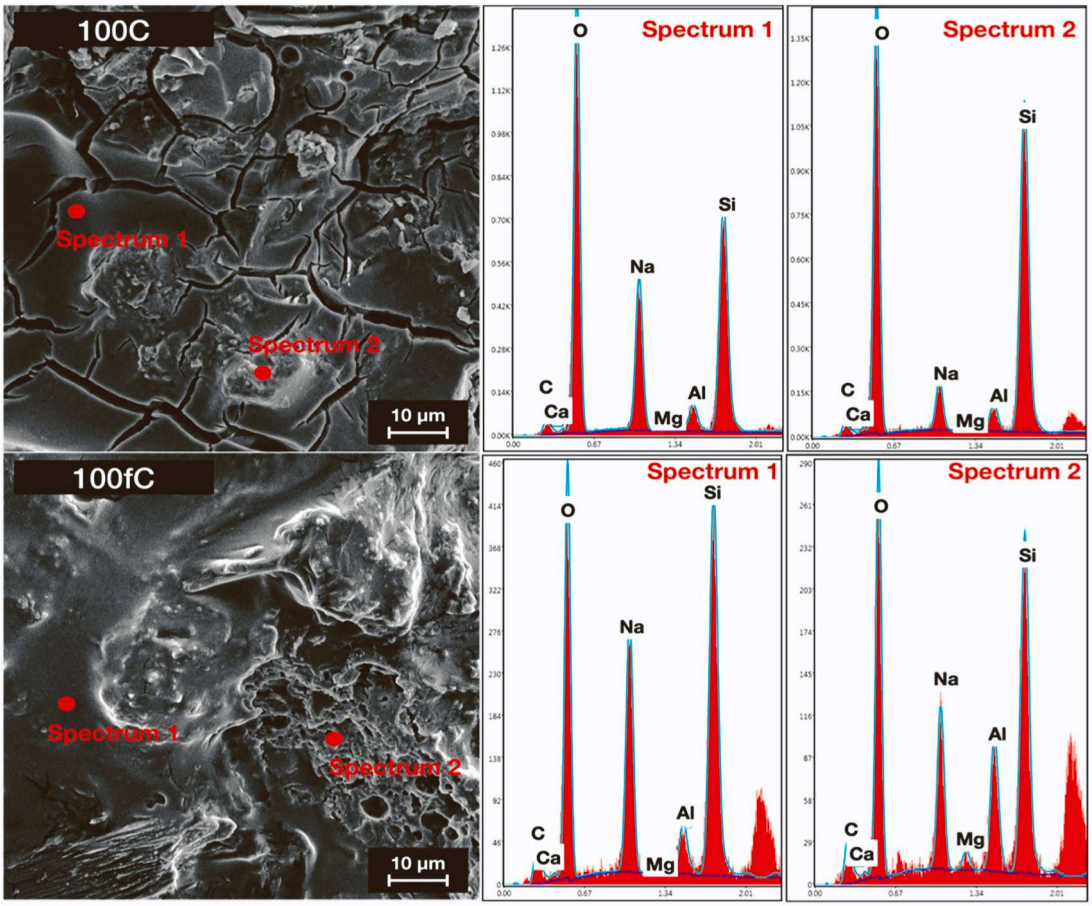

Fig. 9. Micrographs of 100 % CBA geopolymers. Top: raw CBA. Bottom: alkali-fused CBA.

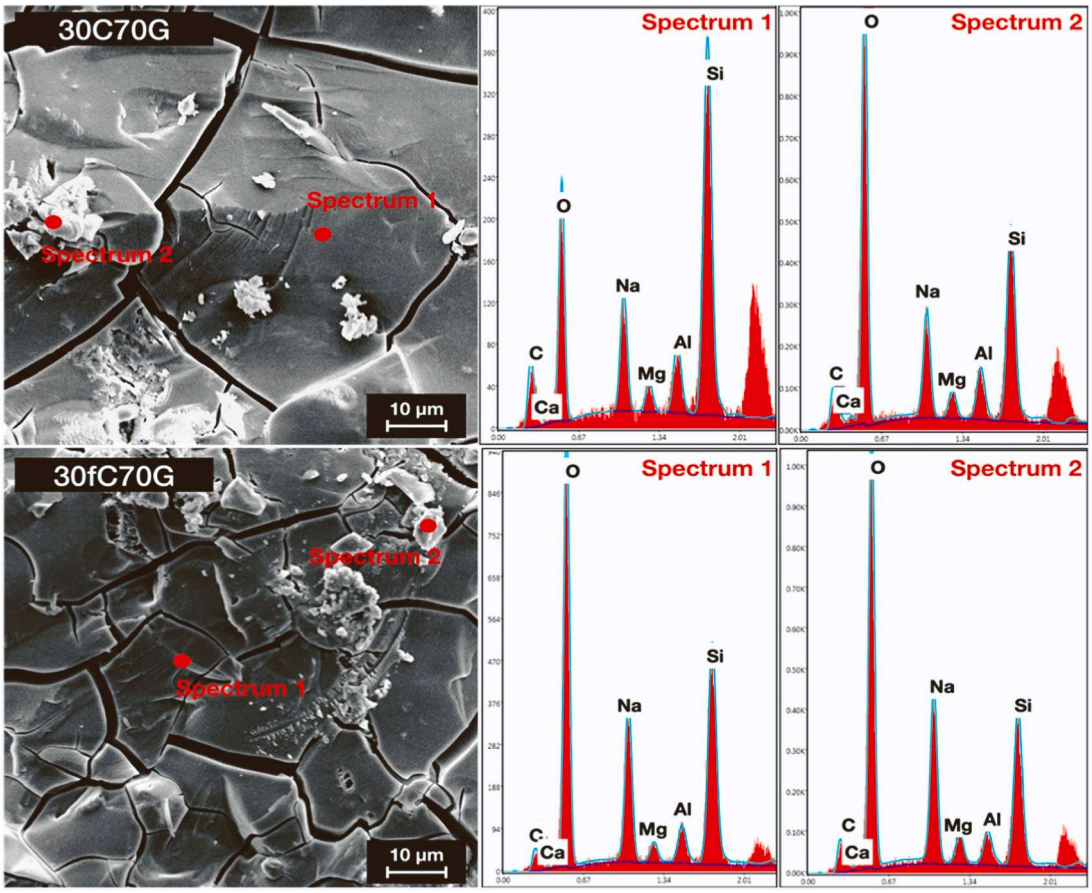

Fig. 10. Micrographs of CBA-GGBS geopolymers. Top: raw CBA. Bottom: alkali-fused CBA.

geopolymers. The EDX analyses (Figs. 9 and 10) revealed high Si and Na content in the vitreous geopolymer suggesting that they are a product of polymerisation consistent with previous authors. The main polymerisation reaction product of low-calcium (aluminosilicate rich) precursors is an alkaline aluminosilicate hydrate gel (N-(A)-S-H) [17,46,51].

In the geopolymers made with 100 % CBA, alkali fusion improved the quality of the matrix by substantially reducing cracking (Fig. 9). An intricate network of cracks, occasionally interconnecting and breaking plates apart, is apparent in the raw CBA geopolymers (100 C) while a denser matrix without obvious cracking appears in the alkali-fused CBA geopolymers (100fC). The vitreous cement of the alkali-fused CBA geopolymer (100fC) consistently shows a higher concentration of Si and Na which agrees with the presence of abundant Si-rich gel that is consistent with the enhanced mechanical performance seen in the strength results above. Particulate clusters appeared sporadically in the raw CBA geopolymer. These are unreacted remnants of CBA particles, as suggested by the high Si and a low Na content evidenced with EDX; and are consistent with the lower reactivity and lower mechanical performance of raw CBA geopolymers evidenced above. The alkali-fusion process significantly improved the reactivity of CBA in geopolymerisation reactions. However, some porous and sponge-like regions appear in the 100fC matrix, presumably unreacted, alkali-fused CBA particles (Fig. 9).

The micrographs of the CBA-GGBS geopolymers are included in Fig. 10. Adding GGBS made the vitreous geopolymer matrices more homogenous and denser, with fewer unreacted particles; however, showing similar cracking. The cracks are due to autogenous unrestrained shrinkage and are typical of alkali activated materials such as geopolymers. The cracking evidenced are shrinkage cracks inherent to the polymerisation process and caused by the loss of water-inducing volume change during polymerisation [50]. Shrinkage cracking is widely found in alkali-activated slag and FA/GGBS geopolymers [65], and it is more prone to occur in low Ca/Si matrices [66].

In the CBA-GGBS geopolymers, the [Ca^{2+}] can transform N-A-S-H geopolymer gel into C-A-S-H gel which increases density and enhances the mechanical performance [67] but can exacerbate shrinkage [68]. Ye & Radlińska [69] also report the collapse and redistribution of C-A-S-H gel leading to significant shrinkage. Furthermore, shrinkage is considered to relate to the content of Na_2O in high Ca systems. The alkali fusion process introduced significant Na^+ which may trigger more intense autogenous shrinkage [70].

The FTIR spectra of the geopolymers and the alkali-fused CBA powder (af-C) appear in Figure. The spectra are dominated by absorption bands located at 800–1200 cm^{-1} which are due to the stretching vibrations of Si-O-Si(Al) [71]. The wide 800–1200 cm^{-1} bands in the CBA powder (af-C) and the CBA geopolymer (100fC) suggest a wide distribution of Si units with varying bonds. In contrast, in the CBA-GGBS geopolymer (30fC70G), the main band is relatively narrow and shifted towards lower wave numbers indicating the substitution of Al into the Si-O-Si structure [48,72]. The absorption band of Si-O-Si(Al) in the CBA-GGBS geopolymer is notably enhanced. This agrees with the significant contribution of GGBS to the geopolymerisation process evidenced in the results above.

The characteristic bands for carbonate occur in the spectral regions 1400–1600 cm^{-1} (v3; asymmetric stretch vibration) and 873–880 cm1 (v2; out-of-plane bend vibration) [73]. Therefore, the bands located at 1350–1550 cm^{-1} are assigned to the anti-symmetric stretching of carbonate. Two distinct patterns were found: a broad band with a nearly symmetrical centre at 1392 cm^{-1} (30fC70G geopolymer) and two sharp bands with asymmetrical centres at 1440 and 1409 cm^{-1} (af-C powder and 100fC geopolymer). The ν_3(CO) stretch mode in 30fC70G is characteristic of free carbonate ions [73]. The presence of free carbonate ions

is attributed to the absorption of atmospheric carbon dioxide by the abundant Ca^{2+} in GGBS. The carbonate bands centred at 1440 and 1409 cm^{-1} (in the af-C powder and 100fC geopolymer) are narrower waves of higher wave numbers. These characteristics indicate that the carbonate is tightly connected to the matrix and may even be bound to it [73]. Therefore, the FTIR results indicate that the GGBS is more reactive than alkali-fused CBA and the Ca and Al in the system also promoted and participated in polymerisation.

4. Conclusion

A crop biomass ash (CBA) collected from a biomass power station was used as a precursor to develop geopolymer. Based on the experimental results above, the conclusions are as follows:

- The geopolymers made with (only) **raw CBA** attained the lowest strengths of 7.46 and 2.99 MPa (compressive and flexural respectively). However, these geopolymers are produced with extremely low carbon emission and environmental impact; and their strength range is suitable for most construction applications unless higher strength is required for load bearing purposes.
- Partially replacing the raw ash with slag raised strength to over 25 MPa and 7 MPa -compressive and flexural respectively.
- **Alkali-fusing the ash** greatly enhanced reactivity, improving polymerisation and increasing strength: the geopolymer made with (only) alkali-fused CBA achieved high strengths of 39.35 and 10.74 MPa - compressive and flexural respectively.
- Even at low temperature (600°C) alkali fusion is an effective method for increasing the strength of CBA geopolymers. Alkali fusion breaks silicate structures as strong and stable as the quartz and feldspar originally comprising the CBA, releasing active radicals that participate in polymerisation reactions forming cementing hydrates that increase the geopolymer strength.
- The geopolymers made with **alkali-fused CBA and GGBS** constantly display outstanding mechanical performance (42–44 MPa compressive strength at 28 d.), and variations in activator composition had no significant impact on mechanical performance.
- The GGBS stabilized the geopolymer system against fluctuations in activator composition. The active Si, Al and Ca released by GGBS participate in the polymerization reaction, increasing geopolymer strength.
- The most alkaline activator compositions ($SiO_2/Na_2O = 1.0$) caused rapid precursor dissolution which produced flash set of the geopolymer.
- The geopolymers show vitreous structures of cementing gels, with high Si^{4+} and Na^{+} contents, consistent with alkaline silico-aluminate hydrate gel (N-(A)-S-H) which is a typical product of polymerisation.
- Incorporating slag amorphized the structure of the geopolymer to a much greater extent than alkali-fusing the ash. However, there is no direct proportionality between increasing vitreousness and improving strength as the geopolymers with crystalline structure (100 % alkali-fused CBA geopolymer) is nearly as strong as the vitreous CBA-GGBS geopolymer (39 vs 44 MPa).
- The FTIR results show ample Si-O-Si(Al) bonds in the geopolymer made with alkali-fused CBA. The presence of GGBS significantly increased the absorption intensity of these bonds, indicating the presence of more abundant C(N)-A-S-H which improved mechanical properties.

In summary, CBA waste has substantial potential as a precursor for developing geopolymers. The incorporation of GGBS in certain proportions enhances the mechanical properties of the ensuing geopolymer. Furthermore, alkali fusion is an effective method to increase the reactivity of CBA, facilitating the preparation of high-performance geopolymers. This research provides a viable method for recycling CBA, thereby adding value to this (otherwise) waste material and contributing to sustainable management in the construction industry.

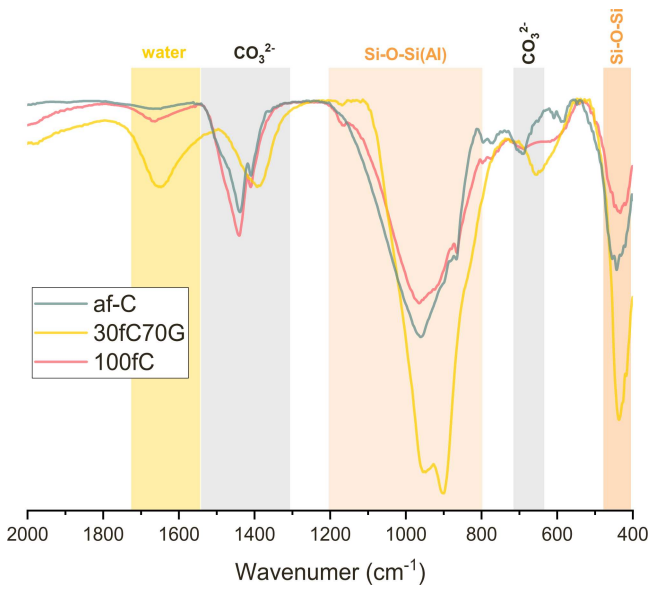

Fig. 11. FTIR spectra of CBA and CBA-GGBS geopolymers and alkali-fused, CBA powder (af-C).

CRediT authorship contribution statement

Sara Pavia: Writing – review & editing, Supervision, Project administration, Investigation, Funding acquisition, Formal analysis, Conceptualization. **Zehao Lei:** Writing – original draft, Resources, Methodology, Investigation, Formal analysis, Data curation, Conceptualization.

Declaration of Competing Interest

The authors declare that they have no known competing financial interests or personal relationships that could have appeared to influence the work reported in this paper.

Data Availability

Data will be made available on request.

Acknowledgements

The authors thank the China Scholarship Council (No. 202007090014) for supporting this research. We thank our technical staff for helping us with testing, especially M. Grimes, P. Veale, M. Gilligan and our Chief Technician D. McCauley.

References

[1] M. Lieder, A. Rashid, Towards circular economy implementation: a comprehensive review in context of manufacturing industry, J. Clean. Prod. 115 (2016) 36–51, https://doi.org/10.1016/j.jclepro.2015.12.042.
[2] J. Kirchherr, D. Reike, M. Hekkert, Conceptualizing the circular economy: an analysis of 114 definitions, Resour. Conserv. Recycl. 127 (2017) 221–232, https://doi.org/10.1016/j.resconrec.2017.09.005.
[3] Y. Geng, B. Doberstein, Developing the circular economy in China: challenges and opportunities for achieving "leapfrog development, Int. J. Sustain. Dev. World Ecol. 15 (2008) 231–239, https://doi.org/10.3843/SusDev.15.3:6.
[4] Z. Yuan, J. Bi, Y. Moriguichi, The circular economy: a new development strategy in China, J. Ind. Ecol. 10 (2006) 4–8.
[5] A. Arrigoni, D.K. Panesar, M. Duhamel, T. Opher, S. Saxe, I.D. Posen, H. L. MacLean, Life cycle greenhouse gas emissions of concrete containing supplementary cementitious materials: cut-off vs. substitution, J. Clean. Prod. 263 (2020) 121465, https://doi.org/10.1016/j.jclepro.2020.121465.

[6] J.L. Easterly, M. Burnham, Overview of biomass and waste fuel resources for power production, Biomass-.-. Bioenergy 10 (1996) 79–92, https://doi.org/10.1016/0961-9534(95)00063-1.
[7] B.K. Sovacool, Energy policymaking in Denmark: implications for global energy security and sustainability, Energy Policy 61 (2013) 829–839, https://doi.org/10.1016/j.enpol.2013.06.106.
[8] R.L. Bain, Electricity from biomass in the United States: status and future direction, Bioresour. Technol. 46 (1993) 86–93, https://doi.org/10.1016/0960-8524(93)90058-J.
[9] A.F. Kirkels, Discursive shifts in energy from biomass: a 30 year European overview, Renew. Sustain. Energy Rev. 16 (2012) 4105–4115, https://doi.org/10.1016/j.rser.2012.03.037.
[10] I. Malico, R. Nepomuceno Pereira, A.C. Gonçalves, A.M.O. Sousa, Current status and future perspectives for energy production from solid biomass in the European industry, Renew. Sustain. Energy Rev. 112 (2019) 960–977, https://doi.org/10.1016/j.rser.2019.06.022.
[11] B. Lin, J. He, Is biomass power a good choice for governments in China? Renew. Sustain. Energy Rev. 73 (2017) 1218–1230, https://doi.org/10.1016/j.rser.2017.02.024.
[12] Z. Zhao, H. Yan, Assessment of the biomass power generation industry in China, Renew. Energy 37 (2012) 53–60, https://doi.org/10.1016/j.renene.2011.05.017.
[13] L. Zhang, C. (Charles Xu, P. Champagne, Overview of recent advances in thermo-chemical conversion of biomass, Energy Convers. Manag. 51 (2010) 969–982, https://doi.org/10.1016/j.enconman.2009.11.038.
[14] S.V. Vassilev, D. Baxter, L.K. Andersen, C.G. Vassileva, An overview of the chemical composition of biomass, Fuel 89 (2010) 913–933, https://doi.org/10.1016/j.fuel.2009.10.022.
[15] S.V. Vassilev, D. Baxter, L.K. Andersen, C.G. Vassileva, An overview of the composition and application of biomass ash. Part 1. Phase–mineral and chemical composition and classification, Fuel 105 (2013) 40–76, https://doi.org/10.1016/j.fuel.2012.09.041.
[16] A.L. Almutairi, B.A. Tayeh, A. Adesina, H.F. Isleem, A.M. Zeyad, Potential applications of geopolymer concrete in construction: a review, Case Stud, Constr. Mater. 15 (2021) e00733.
[17] P. Duxson, A. Fernández-Jiménez, J.L. Provis, G.C. Lukey, A. Palomo, J.S. van Deventer, Geopolymer technology: the current state of the art, J. Mater. Sci. 42 (2007) 2917–2933.
[18] J.L. Provis, J.S.J. Van Deventer, Geopolymers: Structures, Processing, Properties And Industrial Applications, Elsevier, 2009.
[19] P.K. Mehta, Rice husk ash–A unique supplementary cementing material, Adv. Concr. Technol. (1994) 419–443.
[20] P.K. Mehta, Properties of blended cements made from rice husk ash, Acids J. Proc. 74 (1977), https://doi.org/10.14359/11022.
[21] J. Payá, J. Monzó, M.V. Borrachero, L. Díaz-Pinzón, L.M. Ordóñez, Sugar-cane bagasse ash (SCBA): studies on its properties for reusing in concrete production, J. Chem. Technol. Biotechnol. 77 (2002) 321–325, https://doi.org/10.1002/jctb.549.
[22] G.C. Cordeiro, R.D. Toledo Filho, E.M.R. Fairbairn, Effect of calcination temperature on the pozzolanic activity of sugar cane bagasse ash, Constr. Build. Mater. 23 (2009) 3301–3303.
[23] P. Chindaprasirt, S. Rukzon, Strength, porosity and corrosion resistance of ternary blend Portland cement, rice husk ash and fly ash mortar, Constr. Build. Mater. 22 (2008) 1601–1606.
[24] K. Ganesan, K. Rajagopal, K. Thangavel, Rice husk ash blended cement: assessment of optimal level of replacement for strength and permeability properties of concrete, Constr. Build. Mater. 22 (2008) 1675–1683.
[25] A. Sales, S.A. Lima, Use of Brazilian sugarcane bagasse ash in concrete as sand replacement, Waste Manag 30 (2010) 1114–1122.
[26] G.C. Cordeiro, R.D. Toledo Filho, E. de Moraes Rego Fairbairn, Use of ultrafine rice husk ash with high-carbon content as pozzolan in high performance concrete, Mater. Struct. 42 (2009) 983–992.
[27] M. Frias, E. Villar-Cocina, E. Valencia-Morales, Characterisation of sugar cane straw waste as pozzolanic material for construction: calcining temperature and kinetic parameters, Waste Manag 27 (2007) 533–538.
[28] R.L. Figueiredo, S. Pavía, A study of the parameters that determine the reactivity of sugarcane bagasse ashes (SCBA) for use as a binder in construction, SN Appl. Sci. 2 (2020) 1–15.
[29] S. Pavía, R. Walker, P. Veale, A. Wood, Impact of the properties and reactivity of rice husk ash on lime mortar properties, J. Mater. Civ. Eng. 26 (2014) 04014066.
[30] Z. Lei, S. Pavia, X. Wang, Biomass ash waste from agricultural residues: Characterisation, reactivity and potential to develop one-part geopolymer cement, Constr. Build. Mater. 431 (2024) 136544, https://doi.org/10.1016/j.conbuildmat.2024.136544.
[31] S. Ferreiro, M.M.C. Canut, J. Lund, D. Herfort, Influence of fineness of raw clay and calcination temperature on the performance of calcined clay-limestone blended cements, Appl. Clay Sci. 169 (2019) 81–90, https://doi.org/10.1016/j.clay.2018.12.021.
[32] B. Fabbri, S. Gualtieri, C. Leonardi, Modifications induced by the thermal treatment of kaolin and determination of reactivity of metakaolin, Appl. Clay Sci. 73 (2013) 2–10, https://doi.org/10.1016/j.clay.2012.09.019.
[33] Z. Lei, S. Pavia, Potential of spent fluid cracking catalyst (FCC) waste for low-carbon cement production. Effect of treatments to enhance reactivity, Cement 14 (2023) 100081, https://doi.org/10.1016/j.cement.2023.100081.
[34] J.-B.M. Dassekpo, L. Miao, J. Bai, Q. Gong, N.N. Shao, Z. Dong, F. Xing, J. Ye, Phase dissolution and improving properties of completely decomposed granite through alkali fusion method, Cem. Concr. Compos. 127 (2022) 104407, https://doi.org/10.1016/j.cemconcomp.2022.104407.
[35] M.X. Peng, Z.H. Wang, S.H. Shen, Q.G. Xiao, L.J. Li, Y.C. Tang, L.L. Hu, Alkali fusion of bentonite to synthesize one-part geopolymeric cements cured at elevated temperature by comparison with two-part ones, Constr. Build. Mater. 130 (2017) 103–112, https://doi.org/10.1016/j.conbuildmat.2016.11.010.
[36] H. Tchakoute Kouamo, J.A. Mbey, A. Elimbi, B.B. Kenne Diffo, D. Njopwouo, Synthesis of volcanic ash-based geopolymer mortars by fusion method: effects of adding metakaolin to fused volcanic ash, Ceram. Int. 39 (2013) 1613–1621, https://doi.org/10.1016/j.ceramint.2012.08.003.
[37] S.P. Frankoski, S. Siggia, Analysis of carboxylic esters using alkali fusion reaction gas chromatography, Anal. Chem. 44 (1972) 507–511.
[38] D.D. Schlueter, S. Siggia, Analysis of polysiloxanes by alkali fusion reaction gas chromatography, Anal. Chem. 49 (1977) 2343–2348.
[39] M.M. Todand, I. JarviS, K.E. Jarvis, Microwave digestion and alkali fusion procedures for the determination of the platinum-group elements and gold in geological materials by ICP-MS, Chem. Geol. 124 (1995) 21–36, https://doi.org/10.1016/0009-2541(95)00021-D.
[40] J. Mantero, M. Lehritane, S. Hurtado, R. García-Tenorio, Radioanalytical determination of actinoids in refractory matrices by alkali fusion, J. Radioanal. Nucl. Chem. 286 (2010) 557–563.
[41] N. Shigemoto, H. Hayashi, K. Miyaura, Selective formation of Na-X zeolite from coal fly ash by fusion with sodium hydroxide prior to hydrothermal reaction, J. Mater. Sci. 28 (1993) 4781–4786.
[42] T. Wajima, Y. Ikegami, Synthesis of crystalline zeolite-13X from waste porcelain using alkali fusion, Ceram. Int. 35 (2009) 2983–2986, https://doi.org/10.1016/j.ceramint.2009.03.014.
[43] H. Mori, Extraction of silicon dioxide from waste colored glasses by alkali fusion using potassium hydroxide, J. Mater. Sci. 38 (2003) 3461–3468.
[44] M. Tang, C. Zhou, J. Pan, N. Zhang, C. Liu, S. Cao, T. Hu, W. Ji, Study on extraction of rare earth elements from coal fly ash through alkali fusion–Acid leaching, Miner. Eng. 136 (2019) 36–42.
[45] S. Moukannaa, A. Nazari, A. Bagheri, M. Loutou, J.G. Sanjayan, R. Hakkou, Alkaline fused phosphate mine tailings for geopolymer mortar synthesis: thermal stability, mechanical and microstructural properties, J. Non-Cryst. Solids 511 (2019) 76–85, https://doi.org/10.1016/j.jnoncrysol.2018.12.031.
[46] J.L. Provis, J.S. Van Deventer, Alkali Activated Materials: State-of-the-art Report, RILEM TC 224-AAM, Springer Science & Business Media, 2013.
[47] A. Fernández-Jiménez, F. Puertas, Effect of activator mix on the hydration and strength behaviour of alkali-activated slag cements, Adv. Cem. Res. 15 (2003) 129–136.
[48] A. Fernández-Jiménez, F. Puertas, I. Sobrados, J. Sanz, Structure of calcium silicate hydrates formed in alkaline-activated slag: influence of the type of alkaline activator, J. Am. Ceram. Soc. 86 (2003) 1389–1394.
[49] Y.J. Zhang, Y.L. Zhao, H.H. Li, D.L. Xu, Structure characterization of hydration products generated by alkaline activation of granulated blast furnace slag, J. Mater. Sci. 43 (2008) 7141–7147.
[50] F. Pacheco-Torgal, J. Labrincha, C. Leonelli, A. Palomo, P. Chindaprasit, Handbook of Alkali-activated Cements, Mortars and Concretes, Elsevier, 2014.
[51] F. Pacheco-Torgal, J. Castro-Gomes, S. Jalali, Alkali-activated binders: a review: Part 1. Historical background, terminology, reaction mechanisms and hydration products, Constr. Build. Mater. 22 (2008) 1305–1314.
[52] B. Singh, M.R. Rahman, R. Paswan, S.K. Bhattacharyya, Effect of activator concentration on the strength, ITZ and drying shrinkage of fly ash/slag geopolymer concrete, Constr. Build. Mater. 118 (2016) 171–179, https://doi.org/10.1016/j.conbuildmat.2016.05.008.
[53] M. Tuyan, Ö. Andiç-Çakir, K. Ramyar, Effect of alkali activator concentration and curing condition on strength and microstructure of waste clay brick powder-based geopolymer, Compos. Part B Eng. 135 (2018) 242–252, https://doi.org/10.1016/j.compositesb.2017.10.013.
[54] O. Alelweet, S. Pavia, Fitness of a high-calcium slag for the production of alkali activated materials, in: Proc. 1st Int. Conf. Constr. Energy Environ. Sustain.-CEES, 2021: pp. 12–15.
[55] A. Gimelli, A. Luongo, Thermodynamic and experimental analysis of a biomass steam power plant: critical issues and their possible solutions with CCGT systems, Energy Procedia 45 (2014) 227–236.
[56] I. Lecomte, C. Henrist, M. Liégeois, F. Maseri, A. Rulmont, R. Cloots, Micro)-structural comparison between geopolymers, alkali-activated slag cement and Portland cement, J. Eur. Ceram. Soc. 26 (2006) 3789–3797, https://doi.org/10.1016/j.jeurceramsoc.2005.12.021.
[57] R. Walker, S. Pavía, Physical properties and reactivity of pozzolans, and their influence on the properties of lime–pozzolan pastes, Mater. Struct. 44 (2011) 1139–1150, https://doi.org/10.1617/s11527-010-9689-2.
[58] R. Walker, S. Pavia, Behaviour and properties of lime-pozzolan pastes, in: W. Jäger, B. Haseltine, A. Fried, Dresden, July, 2010: pp. 353–362. ⟨https://www.academia.edu/download/76619990/Behaviour_20and_20Properties_20of_20Lime-Pozzolan_20Pastes.pdf⟩ (accessed June 18, 2024).
[59] Y.J. Patel, N. Shah, Enhancement of the properties of Ground Granulated Blast Furnace Slag based Self Compacting Geopolymer Concrete by incorporating Rice Husk Ash, Constr. Build. Mater. 171 (2018) 654–662, https://doi.org/10.1016/j.conbuildmat.2018.03.166.
[60] Y.J. Patel, N. Shah, Development of self-compacting geopolymer concrete as a sustainable construction material, Sustain. Environ. Res. 28 (2018) 412–421, https://doi.org/10.1016/j.serj.2018.08.004.
[61] L. Nishanth, Dr.N.N. Patil, Experimental evaluation on workability and strength characteristics of self-consolidating geopolymer concrete based on GGBFS, flyash

and alccofine, Mater. Today Proc. 59 (2022) 51–57, https://doi.org/10.1016/j.matpr.2021.10.200.
[62] J. Tailby, K.J.D. MacKenzie, Structure and mechanical properties of aluminosilicate geopolymer composites with Portland cement and its constituent minerals, Cem. Concr. Res. 40 (2010) 787–794, https://doi.org/10.1016/j.cemconres.2009.12.003.
[63] A. Antoni, J.G. Herianto, E. Anastasia, D. Hardjito, Effect of adding acid solution on setting time and compressive strength of high calcium fly ash based geopolymer, in: AIP Conf. Proc., AIP Publishing, 2017.
[64] J. Satria, A. Sugiarto, D. Hardjito, Effect of variability of fly ash obtained from the same source on the characteristics of geopolymer, in: MATEC Web Conf., EDP Sciences, 2017: p. 01026.
[65] V.M.E. Lima, P.A. Basto, M.A. Henrique, Y.M.B. Almeida, A.A. de Melo Neto, Optimizing the concentration of Na2O in alkaline activators to improve mechanical properties and reduce costs and CO2 emissions in alkali-activated mixtures, Constr. Build. Mater. 344 (2022) 128185, https://doi.org/10.1016/j.conbuildmat.2022.128185.
[66] X. Zhu, D. Tang, K. Yang, Z. Zhang, Q. Li, Q. Pan, C. Yang, Effect of Ca(OH)2 on shrinkage characteristics and microstructures of alkali-activated slag concrete, Constr. Build. Mater. 175 (2018) 467–482, https://doi.org/10.1016/j.conbuildmat.2018.04.180.
[67] J. Wang, T. Huang, G. Cheng, Z. Liu, S. Li, D. Wang, Effects of fly ash on the properties and microstructure of alkali-activated FA/BFS repairing mortar, Fuel 256 (2019) 115919.
[68] B. Zhang, H. Zhu, P. Feng, P. Zhang, A review on shrinkage-reducing methods and mechanisms of alkali-activated/geopolymer systems: effects of chemical additives, J. Build. Eng. 49 (2022) 104056, https://doi.org/10.1016/j.jobe.2022.104056.
[69] H. Ye, A. Radlińska, Shrinkage mechanisms of alkali-activated slag, Cem. Concr. Res. 88 (2016) 126–135, https://doi.org/10.1016/j.cemconres.2016.07.001.
[70] A.A.M. Neto, M.A. Cincotto, W. Repette, Drying and autogenous shrinkage of pastes and mortars with activated slag cement, Cem. Concr. Res. 38 (2008) 565–574.
[71] M. Criado, A. Fernández-Jiménez, A. Palomo, Alkali activation of fly ash: effect of the SiO2/Na2O ratio: Part I: FTIR study, Microporous Mesoporous Mater. 106 (2007) 180–191, https://doi.org/10.1016/j.micromeso.2007.02.055.
[72] R. García, R.V. de la Villa, I. Vegas, M. Frías, M.S. de Rojas, The pozzolanic properties of paper sludge waste, Constr. Build. Mater. 22 (2008) 1484–1490.
[73] M.E. Fleet, Infrared spectra of carbonate apatites: ν2-region bands, Biomaterials 30 (2009) 1473–1481, https://doi.org/10.1016/j.biomaterials.2008.12.007.